Supplementary Information for

Controlling Optically-Driven Atomic Migration Using Crystal-Facet Control in Plasmonic Nanocavities

Angelos Xomalis [1†*], Rohit Chikkaraddy [1†], Eitan Oksenberg[2], Ilan Shlesinger[2], Junyang Huang [1], Erik C. Garnett[2,3], A. Femius Koenderink[2], Jeremy J. Baumberg[1*]

[1] NanoPhotonics Centre, Cavendish Laboratory, Department of Physics, JJ Thompson Avenue, University of Cambridge, Cambridge, CB3 0HE, United Kingdom

[2]Center for Nanophotonics, AMOLF, Science Park 104, 1098 XG, Amsterdam, The Netherlands

[3]Van der Waals-Zeeman Institute, University of Amsterdam, Science Park 904, 1090 GL, Amsterdam, The Netherlands

Supplementary Text

S1 Activation energy calculations:

The surface energy varies for different crystal facets of Au, as the presence of the nearest atoms affect the energy barrier required for atom mobilisation. An adatom on {111} has 3 neighbours, on {100} 4 and on {110} 5 (one in the second layer underneath).[1] Literature shows that the energy/atom on the different crystal facets is: {111} = 0.611 eV/atom, {100} = 0.895 eV/atom and {110} = 1.321 eV/atom.[2] This allows us to estimate the optical intensity needed to overcome the energy barrier resulting in atom diffusion. Along the same lines as in reference,[3] we estimate the thermal energy U_p available per atom, which is converted into a critical laser intensity I by considering the plasmon absorption cross-section σ_{abs} and the plasmon lifetime τ_p:

$$U_p = I\sigma_{abs}\tau_p$$

Thus, an adatom on the facet {111} needs to overcome a laser intensity threshold of I = 0.73 mW/μm^2 (1.833 eV for NPoM) while for {100} needs I = 1.43 mW/μm^2 (3.58 eV for NCoM). We note that the experimental intensities may slightly vary from our estimations due to atomic scale apexes and steps where the adatom has smaller number of nearest atoms and thus reduced energy barrier. Here we assume that all the energy in one plasmon is given to one adatom.

S2 Large area dark field analysis:

Here, 60 nm globular Au nanoparticles are deposited on 3-mercaptopropionic acid (MPA) coated Au substrates by drop casting. We chose to use 60 nm instead of 80 nm due to NIR shifted (10) mode for sub-nm gaps that will be out of the detection range of our spectrometer (Ocean Optics QE65pro). For large area dark-field measurements, we use an in-house particle tracking code written in Python where correction for chromatic aberration considered as different focal heights (z) spectra collected over a Δz of 5 μm. A typical dark-field spectra distribution shown in Fig. S2 (left) where (10) 'coupled'

mode is visible at 735 nm. More than 600 NPoM plasmonic constructs were measured using a 1s integration time (Fig. S2, right).

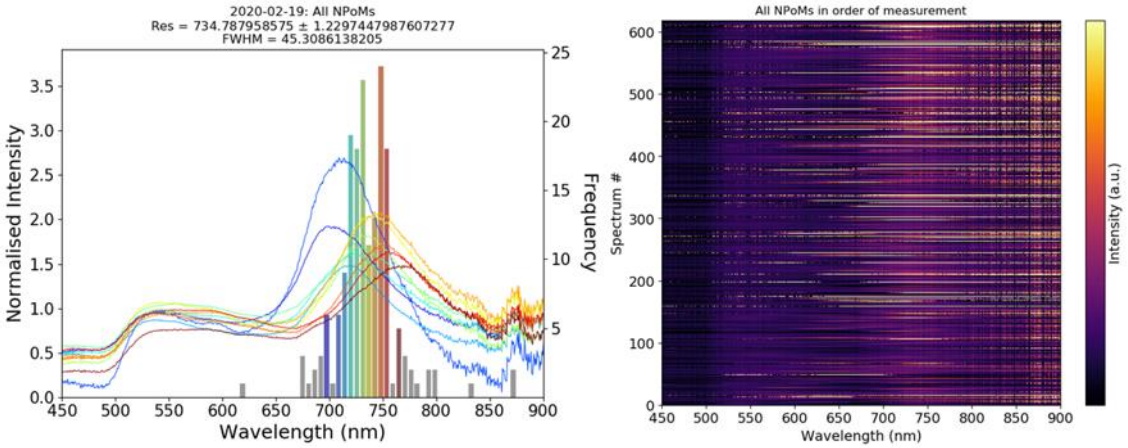

Fig. S2: Dark-field spectra distribution of NPoM plasmonic constructs with MPA as a dielectric spacer. All dark-field spectra are averages (lines) of all spectra and each histogram indicates the occurrence (left). Consecutive dark-field spectra of more than 600 nanoparticles on top of each other (right). Bright (dark) colours correspond high (low) scattering intensity.

From the dark-field scattering modes we can calculate the gap size (d) of the dielectric spacer. Briefly, the scattering (10) mode at 735 nm is hybridization of two sets of modes: the Metal-Insulator-Metal (MIM) cavity modes (S_{0i}) and the nanoparticle antenna modes (l_i). For the cavity modes, which strongly depend on the nanoparticle facet (w) and d size, we use an analytic formula based on the Drude approximation for the resonance position (λ_i):

$$\lambda_i = \lambda_p \sqrt{\frac{w\varepsilon_d}{d\alpha_i} + \varepsilon_\infty},$$

where λ_p is the plasmon wavelength of Au, ε_d the permittivity of the gap spacer, ε_∞ the corresponding Au background permittivity, and α_i the i^{th} antinode of the cylindrical Bessel function that takes into account back-reflection of the cavity modes at the cavity edges.[4] For the nanoparticle antenna modes (l_i) we use the analytic formula based on the circuit model:

$$\lambda_i = \lambda_p \sqrt{2\varepsilon_m + \varepsilon_\infty + 4\varepsilon_m \eta},$$

where ε_m is the permittivity of the surrounding medium and η is the normalised gap capacitance [5]. In this way we calculated d = 0.8 nm for MPA.

S3 BPT powder and NPoM reference measurements:

Here we present bulk powder Raman (black) and SERS (red) spectrum of BPT. SERS spectrum obtained for BPT self-assembled in NPoM geometry. In general, few changes of vibrational modes are attributed to the binding of molecules to gold mirror. Different vibrational energies between the upper and lower benzene ring resulting in splitting of the 1580 cm^{-1} mode.[3] We note that differences between spectra at low wavenumbers (<900 cm^{-1}) may attributed to certain orientation of the molecule within the monolayer that can suppress/enhance specific vibrational modes.

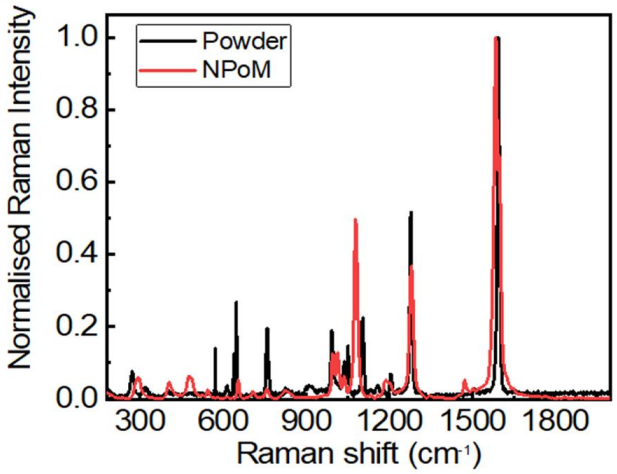

Fig. S3: Comparison of powder Raman and NPoM SERS spectrum for an excitation wavelength of 633 nm.

S4 FDTD near-field simulations:

We obtained finite-difference time-domain (FDTD) simulations for the near-field maps of gap modes of NPoM and NCoM constructs. The Au nanoparticles placed 1.3 nm above an optical thick Au mirror (considering BPT as self-assembled monolayer). The field maps show the different gap modes accommodated into the nm-thick dielectric spacer for the two plasmonic geometries.

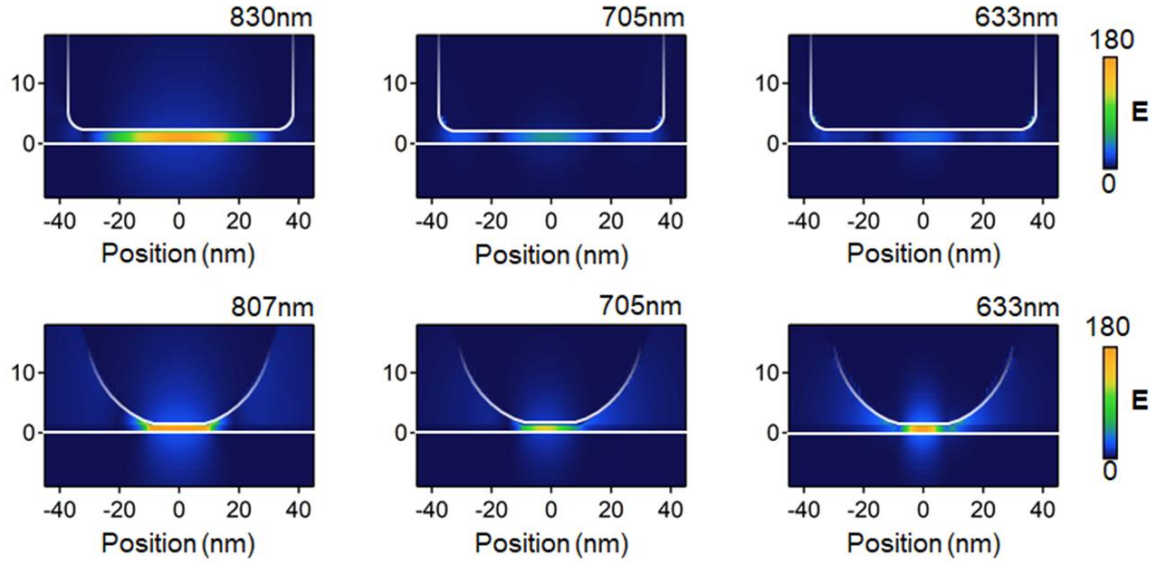

Fig. S4: Nanoconstruct FDTD simulations. Simulated near-field maps of the total electric field (E) for NCoM (top row) and NPoM (bottom row) at a resonance position of their modes. The cube size is 75 nm with 5nm edge rounding and the globular nanoparticle is 80 nm with a 20 nm facet size. The gap size is 1.3 nm with a semi-infinite Au mirror underneath.

S5 DFT simulations:

Density-functional theory (DFT) simulations are performed for the Raman activity of BPT and MPA. For BPT (black) and MPA (green) we considered Au-S bond and molecules in gas phase. Since MPA is in liquid phase at room temperature we performed calculations where MPA considered within

aqueous solution (red). DFT calculations indicate 5-10-fold smaller Raman activity than BPT depending on the surrounding medium.

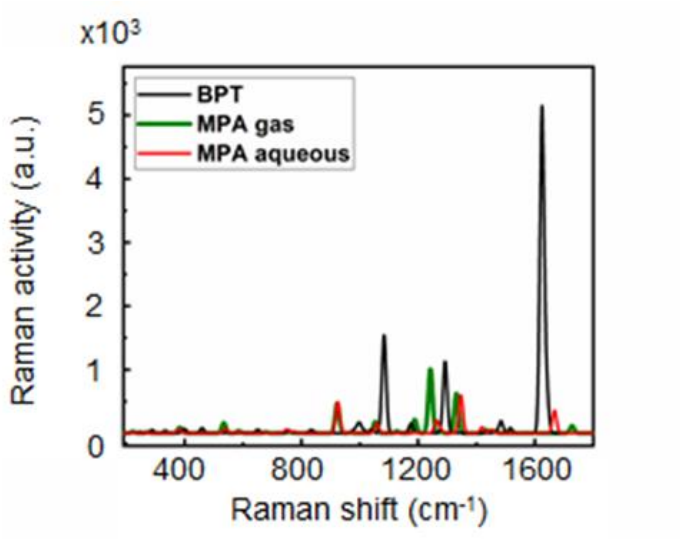

Fig. S5: DFT simulations within different surrounding medium. Raman activity is calculated for BPT (black) and MPA (green) considering bond (Au-S) with substrate and gas phase. In addition, Raman activity is simulated for MPA within aqueous solution (red).

S6 Optical heating simulations:

We carried out photothermal calculations to quantify the effect of local optical heating in the plasmonic nanostructures used in our experiments. We calculate the local optical absorption of the nanoconstructs (using FDTD) and import this into thermal solver (Lumerical) using methods suggested previously.[6] The optical absorption is simulated from an optical intensity of 1 mW/μm^2 at wavelength of 633 nm. In our calculation, we include thermal conductivity of the self-assembled atomic monolayer (0.3 Wm^{-1}K^{-1}) based on previous studies.[7, 8] The NPoMs retain more heat (352 K) than NCoMs (314 K) due to their smaller facet area. Compared to the energies for adatom movement (0.8 eV), these thermal energies are ~25 times smaller so can be neglected in considering direct melting processes.

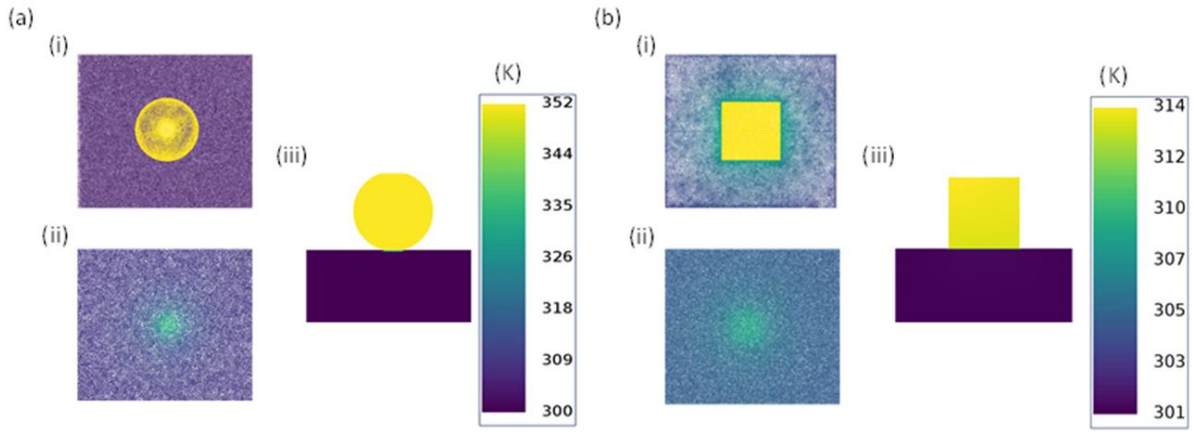

Fig. S6: Local heating calculations on plasmonic nanoconstructs. (a,b) Optically induced heating for NPoM and NCoM nanocavities. (i) Top surface, (ii) 3 nm below the substrate, and (iii) cross-section. Local heating of NPoM reaches 352 K compared to 314 K for NCoM. Ambient temperature is 300 K, irradiation is at 633 nm and optical intensity is 1 mW/μm^2.

Thermal conductivity of the substrate controls the local heating of the nanostructures. To prove this, we repeat the optical heating simulations for an 80 nm Au nanoparticle on SiO_2 substrate *vs* incident power. Our findings are in a good agreement with previous published results,[9] showing how this melts the nanoparticles. The rapid heating is due to the poor thermal conductivity of SiO_2 (1.38 $Wm^{-1}K^{-1}$). In our experiments, the contact to the high thermal conductivity Au substrate greatly reduces such heating. However, the optically-driven adatom diffusion discussed here can be indeed considered as melting of a thin surface layer on the Au, although bulk melting is not observed. Indeed, this surface melting exactly depends on the adatom energy for the different facets.

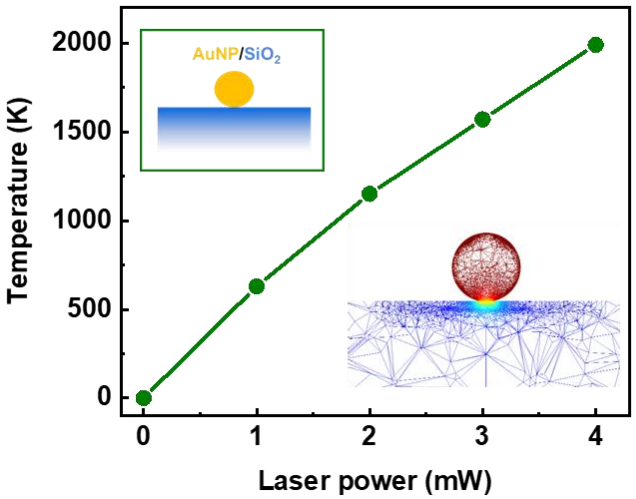

Fig. S7: Heating of Au nanoparticle on SiO_2 substrate. Optical heating of Au nanoparticle (80 nm) *vs* laser power at a wavelength of 633 nm.

References

1. Grzelczak, M.; Pérez-Juste, J.; Mulvaney, P.; Liz-Marzán, L. M., Shape Control in Gold Nanoparticle Synthesis. *Chem. Soc. Rev.* **2008,** *37*, 1783-1791.
2. Vitos, L.; Ruban, A.; Skriver, H. L.; Kollar, J., The Surface Energy of Metals. *Surf. Sci.* **1998,** *411*, 186-202.
3. Benz, F.; Schmidt, M. K.; Dreismann, A.; Chikkaraddy, R.; Zhang, Y.; Demetriadou, A.; Carnegie, C.; Ohadi, H.; De Nijs, B.; Esteban, R., Single-Molecule Optomechanics in "Picocavities". *Science* **2016,** *354*, 726-729.
4. Sigle, D. O.; Mertens, J.; Herrmann, L. O.; Bowman, R. W.; Ithurria, S.; Dubertret, B.; Shi, Y.; Yang, H. Y.; Tserkezis, C.; Aizpurua, J., Monitoring Morphological Changes in 2D Monolayer Semiconductors Using Atom-Thick Plasmonic Nanocavities. *ACS Nano* **2015,** *9*, 825-830.
5. Benz, F.; de Nijs, B.; Tserkezis, C.; Chikkaraddy, R.; Sigle, D. O.; Pukenas, L.; Evans, S. D.; Aizpurua, J.; Baumberg, J. J., Generalized Circuit Model for Coupled Plasmonic Systems. *Opt. Express* **2015,** *23*, 33255-33269.
6. Coppens, Z. J.; Li, W.; Walker, D. G.; Valentine, J. G., Probing and Controlling Photothermal Heat Generation in Plasmonic Nanostructures. *Nano Lett.* **2013,** *13*, 1023-1028.
7. Sergueev, N.; Shin, S.; Kaviany, M.; Dunietz, B., Efficiency of Thermoelectric Energy Conversion in Biphenyl-Dithiol Junctions: Effect of Electron-Phonon Interactions. *Phys. Rev. B* **2011,** *83*, 195415.
8. Sangtarash, S.; Sadeghi, H., Radical Enhancement of Molecular Thermoelectric Efficiency. *Nanoscale Adv.* **2020,** *2*, 1031-1035.

9. Wang, S.; Ding, T., Photothermal-Assisted Optical Stretching of Gold Nanoparticles. *ACS Nano* **2018,** *13*, 32-37.